Boundary Layer Vorticity and the Rise of "Hairpins"

Peter S. Bernard

Abstract The downstream evolution of the vorticity field in the vicinity of hairpin-shaped regions of rotational motion appearing in the transitioning boundary layer is examined. It is shown that the dynamics of hairpins is inseparable from that of the non-rotational vorticity out of which they develop in a self-reinforcing process of ejection and reorientation. Widening the concept of structure to include the complete localized vorticity that produces hairpins, allows for a more complete and self-contained explanation of the boundary layer physics.

1 Introduction

By their nature, boundary layers in high speed flow contain prodigious amounts of vorticity produced at the solid bounding surface by the action of viscosity. A variety of measurement techniques applied to either physical experiments or numerical computations of boundary layers suggest the presence of "coherent" objects within the vorticity field that make essential contributions to the dynamical behavior of the flow. The possibility of arriving at a precise understanding of the boundary layer structure depends on what is meant by "coherency," a concept that is intrinsically difficult to define. In recent times this has come to mean distinctive "regions of rotational motion" and the coherent objects discovered by this criterion are generally hairpin-shaped [1], meaning a flow volume with one or two streamwise oriented "legs" attached to a spanwise "arch."

Since much of the vorticity in the boundary layer does not lie in regions where rotational flow is occurring, the assertion that rotational regions are structures begs the question as to what role the remaining, non-rotational, vorticity has both in the dynamics of the boundary layer in general, and the rotational regions in particu-

Peter S. Bernard
Department of Mechanical Engineering, University of Maryland, College Park, MD 20742, USA,
e-mail: bernard@umd.edu

lar. The importance of this vorticity has been recognized previously, for example in [5] where isosurfaces of spanwise vorticity reveal structural details that conform to the rotational field in the form of hairpins. In addition, several recent studies [2, 3, 4] using a vortex filament scheme visualized vortex structure in the boundary layer without the *a priori* decision that the structures must occupy regions of rotational motion. This showed that hairpin-like regions of rotation have a natural association with uplifting furrow-like folds in the surface vorticity layer that develop downstream into mushroom-like shapes prior to descending into chaotic forms. It is evident from results such as these that there is much to be gained by examining the vorticity environment surrounding individual hairpins with the goal of exposing the role played by all of the vorticity that acts coherently to create the hairpin and that is essential to the physics of the boundary layer. That is the focus of this study.

2 Vortex Filament Scheme

A vortex filament simulation of a spatially growing boundary provides the numerical data for this study. Past work [2, 4] has described the numerical algorithm in detail. It suffices for the present to mention that this is a hybrid approach in the sense that vorticity determined from a finite volume solution to the viscous flow equations on a thin wall mesh is converted to vortex filaments that represent the flow outside the near-wall region. The mesh calculation is both more efficient and accurate at resolving the largely 2D regions of intense vorticity diffusing out of the wall surface than can be achieved using filaments. Within the filament field, hairpin removal provides spatial and temporal intermittent dissipation at inertial range scales as well as limiting growth in the number of vortices. The velocity is calculated using the Biot-Savart law that takes into account the contributions from the vorticity in the mesh and filaments. A velocity potential on the surface triangularization is used to enforce the non-penetration boundary condition.

The simulation considered here occupies a larger spatial region and higher Reynolds number than in previous work [4]. The boundary layer is computed on the top and bottom surfaces of a flat plate with rounded edges of dimensionless length 4 in the streamwise direction, 2.5 in the spanwise direction and 0.05 thick. The region from the front of the plate until $x = 1$ is kept as an inviscid surface so that the boundary layer starts at $x = 1$. Thin regions on the sides and rear of the plate are also taken to be inviscid. The advantage of setting up the flow this way is that it successfully stabilizes the boundary layer against large scale spanwise and wall-normal flow asymmetries that may appear in the unfettered viscous motion past a finite plate.

The Reynolds number at the end of the boundary layer it is $R_e = 225,000$. Just after the start of the viscous computation at $x = 1$ the boundary layer is smooth and is in excellent agreement with the Blasius boundary layer as shown in Fig. 1 comparing the computed velocity field with the Blasius result. Filaments produced in this region are exactly aligned in the spanwise direction. Transition is induced

by the response of the many filaments and vortex elements in the mesh to slight perturbations that are inherent in the discretization of the Biot-Savart law. Though the perturbations are very small initially, and originate entirely within the near-wall mesh, once provoked they grow quickly due to the mutual interactions between vortices. The end result is transition to turbulence, though at Reynolds numbers that are somewhat more typical of a heavily forced flow. For the present simulation this means that the fully turbulent state is achieved at $R_e \approx 100,000$. With finer discretization this trend can be reversed, though at significant increase in the cost of the simulation and without qualitative change in the observed vortex structure.

To obtain information about the vorticity field for this study, the velocity was computed on a fine mesh covering the flow domain and then substituted into second-order accurate finite-difference formulas to get the derivatives needed to compute vorticity. The same data set was used to compute λ_2 whose isosurfaces mark the presence of rotational regions in the flow field including the hairpins.

3 Vorticity and Structure

The filament calculation produces a Klebanoff type transition bridging the gap between the Blasius boundary layer and a fully turbulent flow. This transition mode is marked by the presence of low speed streaks and rotational structures as revealed by λ_2 in the form of hairpins. Figure 2 gives an overhead view of the computed $\lambda_2 = -30$ isosurfaces from $x = 1.4$ until the onset of the fully developed turbulent field. Apart from some noise at the upstream end caused by the locally low amplitude of λ_2 as well as the coarse discretization used in its computation, the visualization of λ_2 reveals Λ-like vortices preceding the formation of rotational regions in the shape of hairpins spaced approximately $\Delta z^+ = 350$ that are not unlike those seen in more traditional grid-based simulations.

To make sense of the vorticity field associated with the appearance of hairpins it is useful to consider the streamwise behavior of the maximum amplitudes of the vorticity components at fixed distances above the wall. Such data is shown in Fig. 3 at a point inside ($y^+ = 24.3$) and a point outside ($y^+ = 51.3$) the near-wall viscous region. In these plots the maxima are restricted to the local spanwise region of a particular Klebanoff streak, in this case the one located between $0.15 \leq z \leq 0.25$. Other

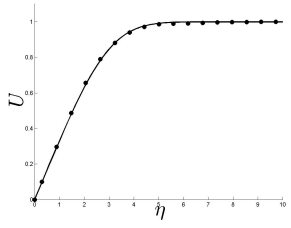

Fig. 1 Velocity in the Blasius region at $x = 1.3$. –, similarity solution; ∘, computed. The similarity variable $\eta = y\sqrt{R_e/(x-0.95)}$ includes a slight adjustment to the virtual origin.

streaks give qualitatively the same result with some small shifting in the streamwise direction. For each figure, the appropriate Blasius spanwise vorticity ω_3 is plotted as a dashed line that shows how the boundary layer would behave in the same location if it had remained laminar. In all cases the turbulent solution departs smoothly from the Blasius values as the flow transitions.

Vertical lines in Fig. 3 indicate three relatively distinct zones in the evolution of the vorticity as it impacts the hairpins. The first region, between $x = 1.4$ and 1.7, is characterized by a steady increase in the streamwise (ω_1) and wall-normal (ω_2) vorticity components near the wall. This is significant if for no other reason than the fact that such non-spanwise vorticity is absent in the Blaisius boundary layer. Downstream of the first zone there commences a number of significant changes to the vorticity amplitudes including a dramatic drop in the magnitude of ω_3 that effectively

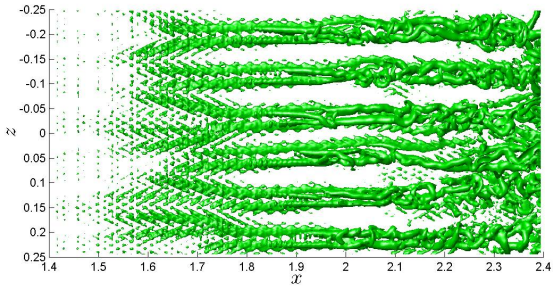

Fig. 2 Overview of $\lambda_2 = -30$ isosurfaces.

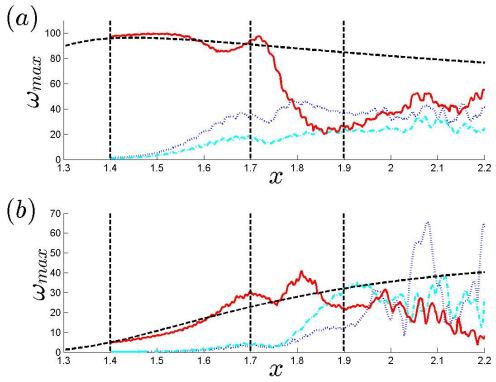

Fig. 3 Streamwise dependence of the maximum vorticity amplitude $0.15 \leq z \leq 0.25$. (a) at $y^+ = 24.3$; (b), $y^+ = 51.3$. ω_1, ($\cdots$, blue); ω_2, ($- \cdot -$, cyan); ω_3, (—, red). Dashed line is the equivalent ω_3 for the Blasius boundary layer.

ends any remaining connection it has to the laminar form. The region $1.7 \leq x \leq 1.9$ is singled out as being distinctive because of the structural transformation accompanying the vorticity behavior in Fig. 3. The end result of the developments in the second zone is to enable the appearance of the fully formed hairpin-like rotational regions located downstream of $x > 1.9$ that characterize transition until the breakdown to fully turbulent flow.

To give more context to the ensuing discussion, the trends in the vorticity magnitude both closer and further from the wall than is considered in Fig. 3 are displayed in Fig. 4. Fig. 4(a) shows that after transition there is a very large increase in the spanwise vorticity at $y^+ = 8.1$ to values much higher than in the equivalent laminar boundary layer. This state persists indefinitely downstream and underlies all the activity that produces turbulent structure. In particular, this reservoir of very high vorticity is undoubtedly the source of all "new" vorticity that enters into the creation of downstream structures after transition. The vorticity trends in Fig. 4(b) at $y^+ = 89.1$ – a region well beyond the direct reach of the viscous boundary layer – shows the last stages in the creation of structure during transition.

Zone 1. The onset of the streamwise structure in Fig. 2 is in the same location as the steady growth in streamwise vorticity near the wall in Fig. 3(a). Upstream of $x = 1.4$ the magnitude of ω_1 is a very slight fraction of the ambient spanwise vorticity, but after $x = 1.4$ it grows significantly becoming more than one third of the magnitude of ω_3 by $x = 1.7$. There is also a somewhat smaller, but non-negligible, rise in wall-normal vorticity accompanying that of ω_1. The location where these vorticity components grow is very close to the boundary, entirely within the viscous region of large spanwise vorticity out of which ω_1 and ω_2 develop by reorientation. The physical boundary no doubt has an influence on suppressing ω_2 in this region.

An idea of the structural form taken by ω_1 as it appears in the flow is given in Fig. 5(a) showing its isosurfaces at four locations in zone 1. The streamwise vorticity has formed into oppositely signed concentrated pairs consistent with the λ_2 isosurfaces in Fig. 2, and is strengthening with downstream distance. Overlying the ω_1 isosurfaces, though not shown, is the smaller wall-normal vorticity.

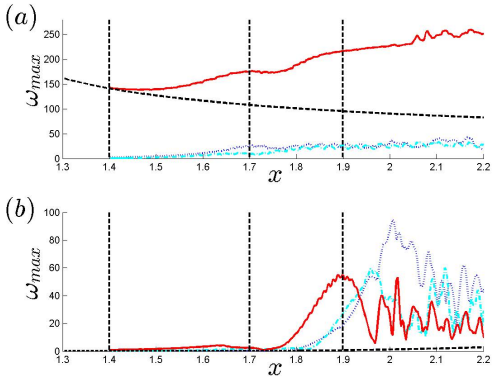

Fig. 4 Streamwise dependence of the maximum vorticity amplitude $0.15 \leq z \leq 0.25$. (a) at $y^+ \approx 8.1$; (b), $y^+ = 89.1$. Definitions of curves are the same as in Fig. 3.

It can be anticipated that there is some loss of ω_3 as ω_1 and ω_2 develop from its reorientation. On the other hand, the counter-rotating velocity created by ω_1 causes significant convection of ω_3 away from the wall. This effect is apparent in Fig. 5(b) giving a visualization of the ω_3 contours at locations in zone 1. Spanwise vorticity decreases near the wall accompanied by its simultaneous rise away from the wall. As the spanwise vorticity is propelled upwards, its place is filled by low speed fluid forming a streak.

The trends in zone 1 of Fig. 3 are consistent with the outward ejection process. For example, in the region just beyond $x = 1.55$ the loss of spanwise vorticity shows up at $y^+ = 24.3$ while at $y^+ = 51.3$ there is a gain. Note, as well, that there is little non-spanwise vorticity at $y^+ = 51.3$ suggesting that the reorientation process that produces such vorticity has yet to rise up to this level above the wall.

Zone 2. Now consider the vorticity trends in Fig. 3 for $1.7 \leq x \leq 1.9$ that is taken to be the second development zone of the structures. A prominent feature is a precipitous drop $-$ to one fifth of its maximum value $-$ of the spanwise vorticity at $y^+ = 24.3$. A significant decrease in ω_3 also occurs at $y^+ = 51.3$, though delayed until $x = 1.8$. Near the wall the streamwise vorticity increases and levels off, while there is a sudden and substantial growth in the wall normal vorticity at $y^+ = 51.3$ until it exceeds the local amplitude of ω_3. The picture that emerges from these trends is that near the wall the reorientation process by which streamwise vorticity develops from ω_3 has run its course. At the same time, the prodigious amount of ejected spanwise vorticity, now outside the near-wall domination of viscous diffusion, rapidly reorients to establish a significant presence of wall-normal vorticity that reaches a good distance from the wall. The latter process is also visible in Fig. 4(b) at points even further downstream where a sudden and significant growth in spanwise vorticity is followed immediately by the production of wall-normal and streamwise vorticity. With its rapid conversion to ω_1 and ω_2 the local dominance of spanwise vorticity ends at these distances from the wall.

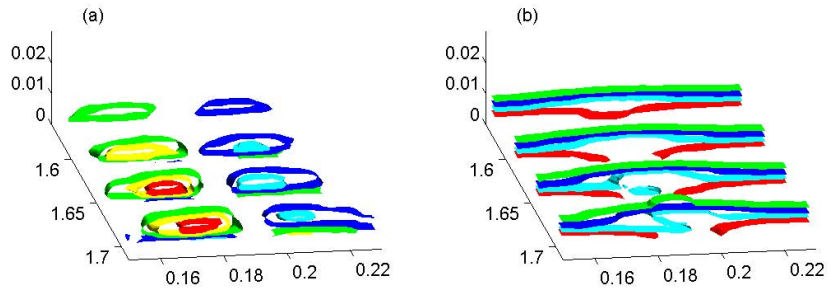

Fig. 5 Isosurfaces of vorticity at several locations in zone 1. (a), green, yellow, red correspond to $\omega_1 = -10, -20, -30$, blue, cyan, magenta are $\omega_1 = 10, 20, 30$ (increasing inwards); (b), green, blue, cyan, red correspond to $\omega_3 = -25, -50, -75, -100$ (increasing towards wall).

Some of the trends in zone 2 are illustrated in the isosurfaces of ω_2 and ω_3 shown in Fig. 6. ω_2 grows to prominence as an oppositely signed pair with a concentration at its upper end coinciding with the λ_2 isosurfaces at the same location. Though not shown, there is a growing presence of ω_1 in this region as well. Figure 6(b) shows that the continued ejection of spanwise vorticity results in its collecting in the region between the counter-rotating motion. Near the wall, ω_3 continues to fall in magnitude even though it strengthens in the fluid sublayer closest to the boundary as seen in Fig. 4(a).

A summary of the state of affairs at the end of zone 2 is given in Fig. 7 that shows, in one plot, isosurfaces of the three vorticity components. Prominent features include the strong streamwise vorticity near the wall that forms a counter-rotating pair, the wall-normal vorticity that has developed outside of the near-wall flow, and finally, the significant spanwise vorticity that collects within the region between the emerging "legs" of the hairpin.

Zone 3. Coincident with $x \approx 1.9$ in Fig. 2 rotational regions with the character of hairpin "legs" emerge out of the λ_2 isosurfaces. Further downstream arch-like structures can be found that cross between the streamwise structures. With increasing x the isosurfaces reveal a breakdown of the rotational regions into a wide range of more complicated rotational forms. A notable aspect of the vorticity maxima in this region, seen in Figs. 3(b) and 4(b), is the development of relatively large sustained peaks in the streamwise vorticity that now dominate the other components. Evidently, this is the vorticity that is responsible for the presence of hairpin "legs," and it appears as the final phase of the conversion of the streamwise vorticity that has been ejecting outwards from the wall.

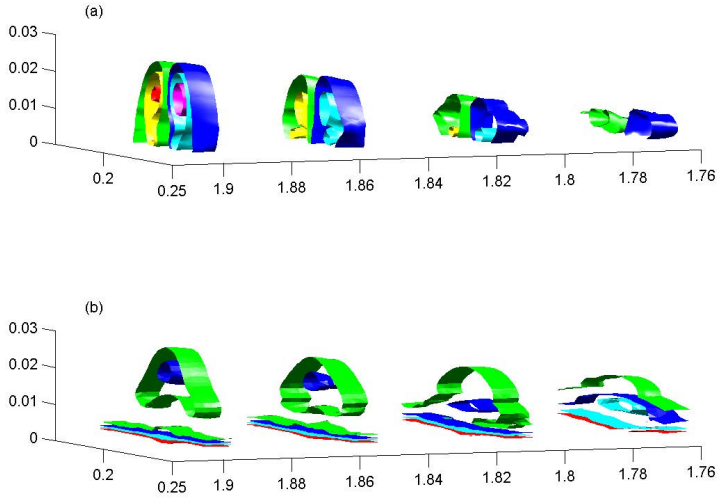

Fig. 6 Isosurfaces of vorticity at several locations in zone 2. (a), green, yellow, red correspond to $\omega_2 = -10, -20, -30$, blue, cyan, magenta are $\omega_2 = 10, 20, 30$ (toward the center); (b), green, blue, cyan, red correspond to $\omega_3 = -20, -45, -70, -95$ (toward the wall).

Previous work that concentrated on examining the vortex filament field in transition [4] showed a direct connection between hairpin "legs" and the lobes of mushroom-shaped structures in the vortex filaments that emerged out of the surface vorticity layer. Such patterns are present among the developing hairpin regions in the current simulation as well, and an example of this is shown in Fig. 8(b). Accompanying this image, in Fig. 8(a), is a view of the isosurfaces of the three vorticity components at the same location. The streamwise vorticity occupies the "legs" that are coincident with the lobes of the filament structure, while the wall-normal vorticity extends upwards through the boundary layer encompassing the stem of the mushroom. Finally, some streamwise vorticity persists at the top of the structure.

An extended streamwise view of the vorticity isosurfaces for this structure is given in Fig. 9 that may be taken as a summary statement of what is entailed in a complete view of the vorticity field associated with hairpins. Spanwise and wall-normal vorticity accompany the prominent counter-rotating streamwise vorticity as a legacy of the mechanisms by which the hairpin-like region developed. It should be emphasized that because the mushroom-like form is unstable it often falls to one side or the other producing single-legged hairpins [4]. For this common occurrence elements of the vorticity arrangement in Fig. 9 are present even if they do not fully resemble the somewhat idealized case depicted here.

Locations above the hairpin "legs" where the spanwise vorticity is concentrated are where the λ_2 signal is likely to indicate the presence of an arch vortex. This agrees with the observation in previous work [3, 4] that the filament field forms concentrated spanwise structure at the locations of arches.

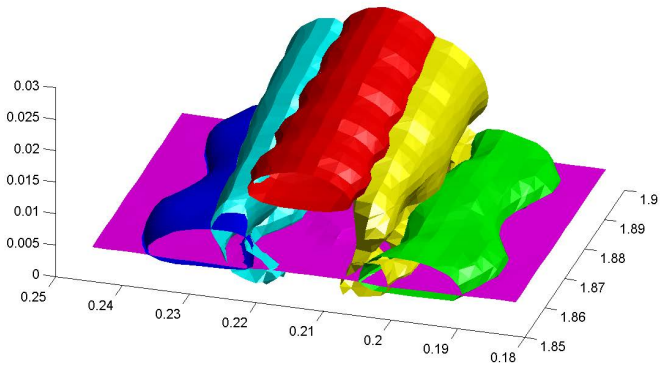

Fig. 7 Isosurfaces of vorticity at the end of zone 2: $\omega_1 = \pm 30$, blue and green; $\omega_2 = \pm 20$, yellow and cyan; ω_3 = -40, red and magenta.

4 Summary and Conclusions

Some essential aspects of the development of the vorticity field in a transitional boundary layer have been examined as it relates to the presence of hairpin-like structures. It is seen that by considering the complete local vorticity field surrounding hairpins, and not focusing exclusively on the rotational motion by which they are defined, the dynamics of the hairpins as well as that of the boundary layer itself can be more clearly understood.

It is found that counter-rotating regions of streamwise vorticity develop in the viscous sub-layer via a self-reinforcing process in which they are strengthened by the spanwise vorticity that they cause to eject. Thus they fuel their own development. As spanwise vorticity extends beyond the viscous sublayer it shears to create wall-normal vorticity that concentrates away from the boundary. Out of this vorticity, streamwise vorticity appears and accumulates to form the hairpins. The ejection process near the wall proceeds until the available spanwise vorticity is depleted. Remnants of the ejected spanwise vorticity, perhaps aided by a roll-up process, persists in the outward flowing regions to produce isosurfaces of rotation that give the impression of arch-type vortices connecting the "legs" of the structures.

A main conclusion is that while it is tempting to view the streamwise isosurfaces of λ_2 as forming hairpin "structure," without also taking into account the active role of the surrounding non-rotational vorticity, the analysis of hairpins misses essential clues to the physics of the boundary layer. For example, the initial appearance of

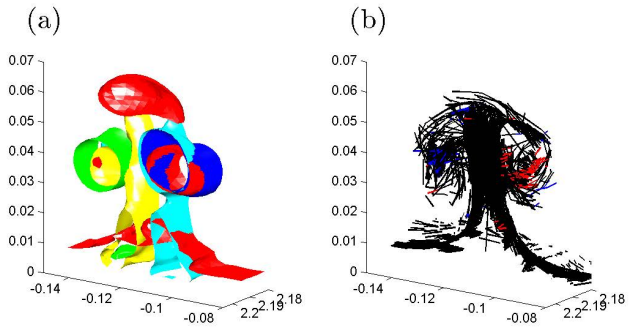

Fig. 8 Comparison of vorticity isosurfaces in a hairpin with the local vortex filament field. (a), isosurfaces: $\omega_1 = \pm 30$, blue and green; $\omega_2 = \pm 15$, yellow and cyan; ω_3 = -15, red; (b), vortex filaments intersecting $2.18 \leq x \leq 2.2$, red and blue filaments are close to the streamwise direction.

streamwise rotation near the wall is only as a perturbation upon the dominant and "invisible" spanwise vorticity field. Downstream, largely missed by λ_2 isosurfaces, is ejecting spanwise vorticity that provides the "fuel" out of which the hairpins appear. Shearing of non-rotational wall-normal and spanwise vorticity explains the emergence of hairpin-shaped rotational regions that constitute just one aspect of a much more intricate vortical structure than is visible as a "hairpin."

After the ejection process depletes spanwise vorticity, it regenerates from the very high vorticity that persists at all times at the wall surface. It is likely that low speed streaks in the fully turbulent region pinpoint locations where some variant of the ejection mechanism described here acts to produce additional vortical structures that work their way to the outer flow. Vortical structures and their remnants accumulate away from the wall and fill out the growing turbulent boundary layer.

Acknowledgements This research was supported in part by the National Science Foundation through XSEDE resources provided by the Pittsburgh Supercomputing Center.

References

1. Adrian, R. J.: Hairpin vortex organization in wall turbulence. Phys. Fluids. **19** 041301 (2007)
2. Bernard, P. S., Collins, P., Potts, M.: Vortex filament simulation of the turbulent boundary layer. AIAA J. **48** 1757-1771 (2010)
3. Bernard, P. S. The hairpin vortex illusion. J. Physics: Conf. Ser. **318** 060024 (2011)
4. Bernard P. S.: Vortex dynamics in transitional and turbulent boundary layers. AIAA J **51** 1828-1842 (2013)
5. Rist, U.: Visualization and tracking of vortices and shear layers in the late stages of boundary-layer laminar-turbulent transition. AIAA Paper 2012-0084 (2012).

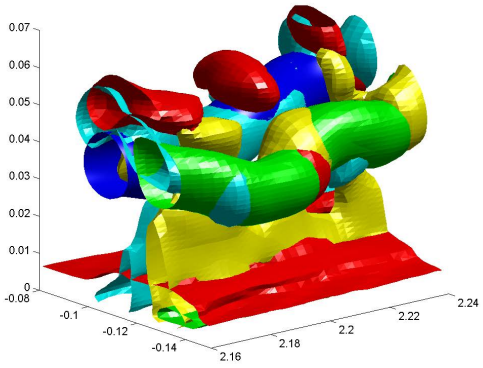

Fig. 9 Isosurfaces of vorticity associated with a hairpin as they develop in zone 3: isosurfaces have the same interpretation as in Fig. 8.